



HAL
open science

The IGR-CaP1 Xenograft Model Recapitulates Mixed Osteolytic/Blastic Bone Lesions Observed in Metastatic Prostate Cancer

Nader Al Nakouzi, Olivia Bawa, Alain Le Pape, Stéphanie Lerondel, Catherine Gaudin, Paule Opolon, Patrick Gonin, Karim Fizazi, Anne Chauchereau

► **To cite this version:**

Nader Al Nakouzi, Olivia Bawa, Alain Le Pape, Stéphanie Lerondel, Catherine Gaudin, et al.. The IGR-CaP1 Xenograft Model Recapitulates Mixed Osteolytic/Blastic Bone Lesions Observed in Metastatic Prostate Cancer. *Neoplasia*, 2012, 14 (5), pp.376-IN1. 10.1593/neo.12308 . hal-03211006

HAL Id: hal-03211006

<https://hal.science/hal-03211006>

Submitted on 28 Apr 2021

HAL is a multi-disciplinary open access archive for the deposit and dissemination of scientific research documents, whether they are published or not. The documents may come from teaching and research institutions in France or abroad, or from public or private research centers.

L'archive ouverte pluridisciplinaire **HAL**, est destinée au dépôt et à la diffusion de documents scientifiques de niveau recherche, publiés ou non, émanant des établissements d'enseignement et de recherche français ou étrangers, des laboratoires publics ou privés.

The IGR-CaP1 Xenograft Model Recapitulates Mixed Osteolytic/Blastic Bone Lesions Observed in Metastatic Prostate Cancer^{1,2}

Nader Al Nakouzi^{*,†}, Olivia Bawa^{†,‡}, Alain Le Pape^{§,#},
Stéphanie Lerondel[§], Catherine Gaudin^{*,†},
Paule Opolon^{†,‡}, Patrick Gonin^{†,¶}, Karim Fizazi^{*,†,**}
and Anne Chauchereau^{*,†}

*Prostate Cancer Group, INSERM U981, Institut Gustave Roussy, Villejuif, France; [†]University Paris-Sud 11, France; [‡]Experimental Pathology Unit of IRCIV, Institut Gustave Roussy, Villejuif, France; [§]UPS44 TAAM-CIPA, CNRS, Orléans, France; [#]INSERM U1100/EA 6305, Faculty of Medicine, Tours, France; [¶]Animal and Veterinary Resources, Institut Gustave Roussy, Villejuif, France; ^{**}Department of Cancer Medicine, Institut Gustave Roussy, Villejuif, France

Abstract

Bone metastases have a devastating impact on quality of life and bone pain in patients with prostate cancer and decrease survival. Animal models are important tools in investigating the pathogenesis of the disease and in developing treatment strategies for bone metastases, but few animal models recapitulate spontaneous clinical bone metastatic spread. In the present study, IGR-CaP1, a new cell line derived from primary prostate cancer, was stably transduced with a luciferase-expressing viral vector to monitor tumor growth in mice using bioluminescence imaging. The IGR-CaP1 tumors grew when subcutaneously injected or when orthotopically implanted, reconstituted the prostate adenocarcinoma with glandular acini-like structures, and could disseminate to the liver and lung. Bone lesions were detected using bioluminescence imaging after direct intratibial or intracardiac injections. Anatomic bone structure assessed using high-resolution computed tomographic scans showed both lytic and osteoblastic lesions. Technetium Tc 99m methylene diphosphonate micro single-photon emission computed tomography confirmed the mixed nature of the lesions and the intensive bone remodeling. We also identified an expression signature for responsiveness of IGR-CaP1 cells to the bone microenvironment, namely expression of CXCR4, MMP-9, Runx2, osteopontin, osteoprotegerin, ADAMTS14, FGFBP2, and HBB. The IGR-CaP1 cell line is a unique model derived from a primary tumor, which can reconstitute human prostate adenocarcinoma in animals and generate experimental bone metastases, providing a novel means for understanding the mechanisms of bone metastasis progression and allowing preclinical testing of new therapies.

Neoplasia (2012) 14, 376–387

Introduction

Prostate cancer (PCa) is the most commonly diagnosed cancer in men in the Western world and is the second leading cause of male cancer deaths [1]. PCa has a high propensity to metastasize to bone, and virtually all patients who die of PCa have bone metastases [2]. Patients with bone metastases experience severe pain, nerve compression syndromes, and pathologic fractures. PCa that has metastasized to bone remains incurable, and in most patients, a fatal outcome is linked to bone metastases rather than to the primary tumor [3]. Although bone metastases are particularly difficult to target, the knowledge of tumor progression and metastasis has recently improved with the emergence

Address all correspondence to: Anne Chauchereau, PhD, Prostate Cancer Group, INSERM U981, Institut Gustave Roussy, 114 rue Edouard Vaillant, Villejuif, F-94805, France. E-mail: anne.chauchereau@igr.fr

¹N.A.N. was supported by the Association pour la Recherche sur le Cancer and the Mutuelle Bleue. The new IGR-CaP1 cell line was the subject of an international patent pending entitled, "Prostate cancer cell lines and their use in screening method," and deposited on the April 14, 2009. Biologic material has been deposited at the Pasteur Institute (Paris) (CNCM I-4126). The patented material will be available under a Material Transfer Agreement for research use.

²This article refers to supplementary materials, which are designated by Figures W1 and W2 and are available online at www.neoplasia.com.

Received 6 February 2012; Revised 18 April 2012; Accepted 18 April 2012

Copyright © 2012 Neoplasia Press, Inc. All rights reserved 1522-8002/12/\$25.00
DOI 10.1593/neo.12308

of new bone-specific therapies. However, the survival benefit of these new bone-specific agents is unclear, and understanding the mechanisms of tumor metastasis remains a challenge. These challenges are obstacles to improving cancer treatment and prognosis.

Under normal conditions, bone undergoes continuous remodeling in a tightly coordinated and balanced process of osteoclast-mediated bone resorption and osteoblast-mediated bone formation. The skeletal-related events associated with bone metastasis are mediated by an imbalance between osteoblasts and osteoclasts that is induced by tumor cells [4,5]. Prostate tumor cells in the bone environment begin to secrete several factors associated with bone remodeling. Some of these factors have osteogenic properties, including the bone morphogenetic proteins and endothelin 1. Other factors, such as parathyroid hormone-related protein, trigger inhibition of osteoblast growth. Additional factors indirectly enhance bone production (e.g., transforming growth factor β), enhance osteosclerosis (e.g., osteoprotegerin [OPG]) or directly initiate osteoclastogenesis (e.g., receptor activator of nuclear factor κ B [RANK] and RANK ligand [RANKL]). In PCa, bone metastases are primarily osteoblastic; however, high bone turnover and consequent excessive bone resorption are also characteristic features of the disease [6].

The molecular mechanisms underlying the bone tropism of PCa metastasis remain unclear. This gap in knowledge is partly due to difficulties both in obtaining metastatic tissue from patients and in generating mouse models that display bone metastasis. Preclinical models are needed to investigate this mechanism and to constitute a useful niche for proof of concept in preclinical evaluations of new therapies. The most popular current models are the PC-3, LNCaP, and DU145 cells and their derived sublines. Although these cell line models represent a major advance in the field of PCa research, they have several inherent drawbacks. In particular, the multistep development of cancer in xenografts remains far from the physiologic reality because most xenografted tumors and tumor cell lines selectively represent the histologic diagnosis and the metastatic patterns of human tumors at an advanced stage. Moreover, few *in vivo* models mimic the natural progression and dissemination of PCa. For example, the PC-3 preclinical model generates only osteoclastic lesions [7]. Indeed, few models reproduce osteoblastic or mixed osteolytic/blastocytic lesions when implanted in the bones of immunocompromised mice, corresponding to the most frequent phenotype in patients. To date, these models are limited to the LNCaP-derived C4-2B, LuCaP 23.1, LAPC9, MDA-PCa-2b, VCaP, and 22Rv1 preclinical models [8–17]. Dynamically monitoring the metastatic development with imaging technology, such as bioluminescence imaging (BLI), currently provides a tremendous advantage for studying bone metastases in xenograft models. The luciferase-expressing PC-3-derived cell lines were the most widely used models [18]. However, the availability of luciferase-expressing models to achieve the follow-up of bone metastasis development using BLI remains quite limited to other models. Indeed, some of these models cannot be grown in culture as LAPC9 and LuCaP series. Thus, new animal models that more closely mimic the human disease are required for a better understanding of the molecular mechanisms of PCa bone metastasis and preclinical research.

Unlike many other cell lines that have been obtained from prostate tumor metastases, the IGR-CaP1 cell line was established from a localized epithelial PCa, which makes it a better model to reflect the mechanisms of tumor progression from localized cancer to metastatic disease. In this report, we describe the establishment of the new IGR-CaP1 preclinical model, which can reconstitute human prostate

adenocarcinoma in animals. We have engineered these cells to express firefly luciferase for visualizing the development of metastases and showed that this model grew in bone after either intratibial injection or inoculation of cells into the left cardiac ventricle of nude mice. We identified a signature of genes that are overexpressed in tumor cells during the bone remodeling process. Thus, this model provides a novel means for identifying and understanding mechanisms that contribute to bone metastasis and allows for preclinical testing of new anticancer therapies, specifically bone-targeting therapies.

Materials and Methods

Cell Lines

The human androgen-independent IGR-CaP1 cell line was established in the laboratory from a primary PCa [19]. PC-3 cell line was purchased from ATCC-LGC (Molsheim, France). Cells were grown in RPMI medium containing 10% fetal bovine serum (PAA Laboratories, Les Mureaux, France) and antibiotics under standard culture conditions.

Retroviral Vector Production and Transduction of IGR-CaP1 Cells

To obtain the IGR-CaP1-Luc cells, we used a retrovirus expressing the luciferase gene (pMEGIX-Luc vector), kindly provided by Dr J.L. Villeval (UMR 1009; Villejuif, France), carrying an expression cassette encoding the firefly luciferase and green fluorescent protein (GFP) genes separated by an internal ribosomal entry site. The Luc-GFP viruses were produced by transient transfection of 293T cells according to standard protocols [20]. Briefly, subconfluent 293T cells were cotransfected with 20 μ g of the luciferase-expressing plasmid vector, 13 μ g of pCMV-Gag-Pol, and 7 μ g of pVSVG by calcium phosphate precipitation. After 16 hours, the culture medium was changed, and the recombinant retrovirus was harvested 48 hours later. For transduction, viruses were added to cells for 24 hours. The GFP-positive IGR-CaP1 luciferase-expressing cells were sorted for green fluorescence using a MoFlo cell sorter (Beckman-Coulter, Miami, FL) before amplification.

Animal Tumor Models

All animal experiments were approved by the local ethics committee (CEEA IRCIV/IGR no. 26, registered with the French Ministry of Research) and were in compliance with EU Directive 63/2010. IGR Animal Resources holds a National Institutes of Health-Department of Health and Human Services Animal Welfare Insurance (no. A5660-01) and is in compliance with the Guide for the Care and Use of Laboratory Animals. Six-week-old male athymic nude mice (*NC-nu/nu*) were purchased from Janvier (Le Genest-St-Isle, France). IGR-CaP1 cells (10^7) were implanted subcutaneously in the right rear flank region of nude mice without Matrigel. For orthotopic injections, IGR-CaP1-Luc cells (10^6) in 20 μ l of phosphate-buffered saline (PBS) were injected after exposure into the prostatic lobe at the base of the seminal vesicles through a midline laparotomy incision as previously described [15]. Tumor size resulting from subcutaneous xenograft was measured with calipers. The following formula was used to calculate tumor volumes: $V = \pi/6 \times L \times l^2$, where L is the length of the longest aspect of the tumor and l is the length of the tumor perpendicular to L . Bioluminescence imaging was used to follow the tumor growth of intraprostatic tumors. The mice were killed, and tumors were excised and measured.

Experimental Metastasis Model

For the intratibial and intracardiac injections, mice were maintained under isoflurane anesthesia during the injection procedure. A 29-gauge needle was inserted extracapsularly through the tibial crest, the epiphysis, and the growth plate. IGR-CaP1-Luc cells (5×10^5 cells in 100 μ l of PBS) were injected in the bone marrow space of the right tibia. The left tibias were either not injected or injected with PBS alone as precise to serve as controls and to evaluate the effect of injection trauma on bone remodeling. Animals were monitored the day after injection and for 5 weeks after injection of IGR-CaP1-Luc cells. After the mice were killed, the tumors and contralateral tibias were harvested. For intracardiac injections, IGR-CaP1-Luc cells (5×10^5) were suspended in 100 μ l of 5% sterile glucose solution and were injected into the left ventricle using a 29-gauge needle after confirmation of the location of the tip of the needle in the left ventricle as indicated by pulsatile blood flow in the hub of the needle. Animals were monitored the day after injection and for 5 weeks after injection of IGR-CaP1-Luc cells.

Bioluminescence Imaging

Mice were injected intraperitoneally with D-luciferin potassium salt (Caliper Life Sciences, Hopkinton, MA) (15 mg/ml in sterile water) 15 minutes before being imaged. The mice were anesthetized with 2% isoflurane and were imaged in dorsal and ventral positions using an IVIS 50 cooled charge-coupled device camera system (Caliper Life Sciences) to monitor tumor growth and metastases dissemination. After acquiring a grayscale photograph, a bioluminescent image was obtained with a 12-cm field of view, a binning (resolution) factor of 8, and a 1/*f* stop-and-open filter. Regions of interest were defined manually (using a standard area in each case), and signal intensities were calculated with Living Image software (Caliper Life Sciences) and expressed as photons per second. Background photon flux was defined from a region of interest drawn over a control.

Micro X-ray Computed Tomography

Mice were anesthetized with a mixture of ketamine (100 mg/kg) and xylazine (10 mg/kg) and were imaged using a micro-computed tomography (CT 120; General Electric, Buc, France). During imaging, 360-degree x-ray projections were collected in 1-degree increments (80 kVp, 450 μ A, 120 milliseconds of exposure time for approximately 25 minutes of total scan time). Projection images were preprocessed and reconstructed into three-dimensional volumes (10,243 voxels; resolution, 93 μ m) on a four-PC reconstruction cluster using a modified tent-FDK cone beam algorithm (GE reconstruction software). Three-dimensional data were processed and rendered (isosurface/maximum intensity projections) using MicroView (GE Healthcare, Milton, Canada). Data analysis was performed first on individual slices (axial, coronal, and sagittal) and then on three-dimensional reconstructed volumes.

Single-Photon Emission Computed Tomography

Methylene diphosphonate (MDP) is a conventional bone scintigraphy agent widely used for functional imaging of bone remodeling, which reflects bone blood flow and osteoblastic activity. MDP is tagged with technetium Tc 99m to generate ^{99m}Tc-MDP, which selectively concentrates in the bone via its chemical adsorption to the crystalline structure of hydroxyapatite. Mice were injected in the tail vein with 18 MBq of ^{99m}Tc-MDP, and images were recorded 60 minutes after

injection. Mice were anesthetized with 1.5% to 2% isoflurane in oxygen and were transferred onto the warmed bed of a NanoSPECT/CT (Bioscan, Washington, DC), a small animal imaging system based on multiplexed multipinhole technology to preserve both sensitivity and resolution. This device incorporates parallel helical CT scanning. Image acquisition parameters were 24 projections and 30 to 60 sec/image, depending on the activity. A dedicated software (InVivoScope 1.39) was used to reconstruct three-dimensional single-photon emission computed tomography (SPECT)/CT fusion images and to quantify radioactivity. Image analysis was performed both qualitatively by comparing the fusion images with bioluminescence and CT data and quantitatively by assessing radioactivity in volumes of interest drawn around tumors in both legs. The results are expressed as percent of injected doses. *P* < .05 was considered statistically significant.

Immunohistochemistry

After imaging, the tissue specimens were collected and fixed in Finefix (Milestone Medical, Bergamo, Italy). The fixed skeleton specimens were decalcified with the Sakura TDE 30 decalcifier system (Sakura, Japan) for 30 to 90 minutes, according to the type of bone. Decalcified femur, tibia, skull, and the lower half of the spine were embedded in paraffin after tissue processing. All long bones were cut sagittally and along a longitudinal axis through the center of each bone. The spines were cut along the anterior-posterior axis. Skulls were also sagittally dissected from the midline. Serial 4- μ m paraffin sections were processed and routinely stained with hematoxylin-eosin-safranin (HES). Tumor and organ sections were incubated with mouse monoclonal antivimentin (clone V9; Dako, Trappes, France), rabbit polyclonal anti-P504S/AMACR (Diagnostic BioSystems, Nanterre, France), rat antimouse CD34 antibody (1:20; Hycult Biotechnology, Nanterre, France), mouse monoclonal anti-Runx2 (27-K; Santa Cruz, Nanterre, France), or rabbit polyclonal anti-MMP-9 (Cell Signaling, Saint Quentin Yvelines, France) antibodies. Immunostaining was visualized using rabbit or mouse PowerVision Kit (ImmunoVision Technologies, Burlingame, CA). Immunohistologic signals were finally revealed with the peroxidase/diaminobenzidine chromogenic substrate. All sections were analyzed using a Zeiss Axiophot microscope (Zeiss, Oberkochen, Germany), and images were acquired with a SensiCam PCO digital camera (PCO, Kelheim, Germany).

TaqMan Real-time Quantitative Reverse Transcription-Polymerase Chain Reaction Analysis

Reverse transcription-polymerase chain reaction (RT-PCR) was performed to confirm the expression of bone metastasis-specific markers in intratibial-injected mice. Total RNA was extracted from bone (9 weeks after inoculation) or tumors tissues (27 weeks after inoculation) using the TriReagent protocol (Invitrogen-life Technologies, Saint Aubin, France), and 5 μ g of RNA was reversed transcribed using random hexamers (Applied Biosystems-life Technologies, Saint Aubin, France). Quantitative RT-PCR was performed with the ABI Prism 7900 Sequence Detection System (Applied Biosystems) using 5 μ l of 1:20 diluted complementary DNA in a final volume of 25 μ l according to the manufacturer's recommendations. The primer/probe sets were obtained from Applied Biosystems (HBB, Hs00758889_s1; TNFRSF11B/OPG, Hs00900358_m1; SPP1/osteopontin, Hs00959010_m1; CXCR4, Hs00607978_s1; ADAMTS14, Hs01548449_m1; FGF2, Hs00230605_m1) and were used according to the manufacturer's recommendations. The amount of sample RNA was normalized

to the amplification of an internal human control (GAPDH-435293E; Applied Biosystems). In each experiment, the relative quantification of the transcripts was derived using the $\Delta\Delta C_T$ method and was expressed relative to the Universal Human Reference RNA (Agilent Technologies, Massy, France). The results were compared with the results from total RNA extracted from subcutaneous xenografts.

Results

Time Course Progression of IGR-CaP1 Tumors

Tumors grew after subcutaneous injection of IGR-CaP1 cells in athymic nude mice (Figure 1A). Subcutaneous xenografts were palpable 2 weeks after injection, with a tumor take of 100% (20 mice). Tumors started to grow at week 3; tumors of $\sim 300 \text{ mm}^3$ were obtained after 6 weeks, and they reached a maximum size of $\sim 500 \text{ mm}^3$ after 15 weeks.

In an effort to specifically follow the tumor growth of intraprostatic tumor noninvasively via BLI, we generated a luciferase- and GFP-expressing IGR-CaP1 cell line by retroviral transduction. Forty-eight hours after transduction, GFP-positive cells were sorted and amplified. GFP-positive, luciferase-expressing cells were inoculated into the prostate of nude mice, and tumor growth was followed for 40 weeks

using BLI. The tumor take was 84% (28/33 mice). The mice were scanned every 3 to 4 weeks. In a group of nine implanted mice, we observed a slow increase in bioluminescence activity that was significant 9 weeks after inoculation and reached a plateau after 30 weeks (Figure 1, B and C). Prostate tumors were confirmed after excision from the euthanized animal at the end of the experiment. At 40 weeks after engraftment in the prostate, the tumor size reached to a maximum of 500 mm^3 . Whereas the IGR-CaP1 cells grew quickly *in vitro*, the tumor growth rate was slower in the animals, especially in orthotopically implanted tumors. This situation most closely reflects the slow clinical progression of PCa.

Reconstitution of Prostate Adenocarcinoma

PC-3 cells are the most commonly used PCa model able to mimic bone metastases [21]. These cells produce highly tumorigenic non-differentiated tumors by 4 weeks when injected subcutaneously. Compared with PC-3 cells with inconspicuous stromal regions, the IGR-CaP1 cells produce more differentiated tumors with glandular acini-like structures suggestive of adenocarcinoma (Figure 2A, *insert* and *arrows*). After direct injection of IGR-CaP1 cells into the prostate, orthotopic tumors were relatively undifferentiated but retained acinar structures and abundant stroma, exhibiting areas of poorly

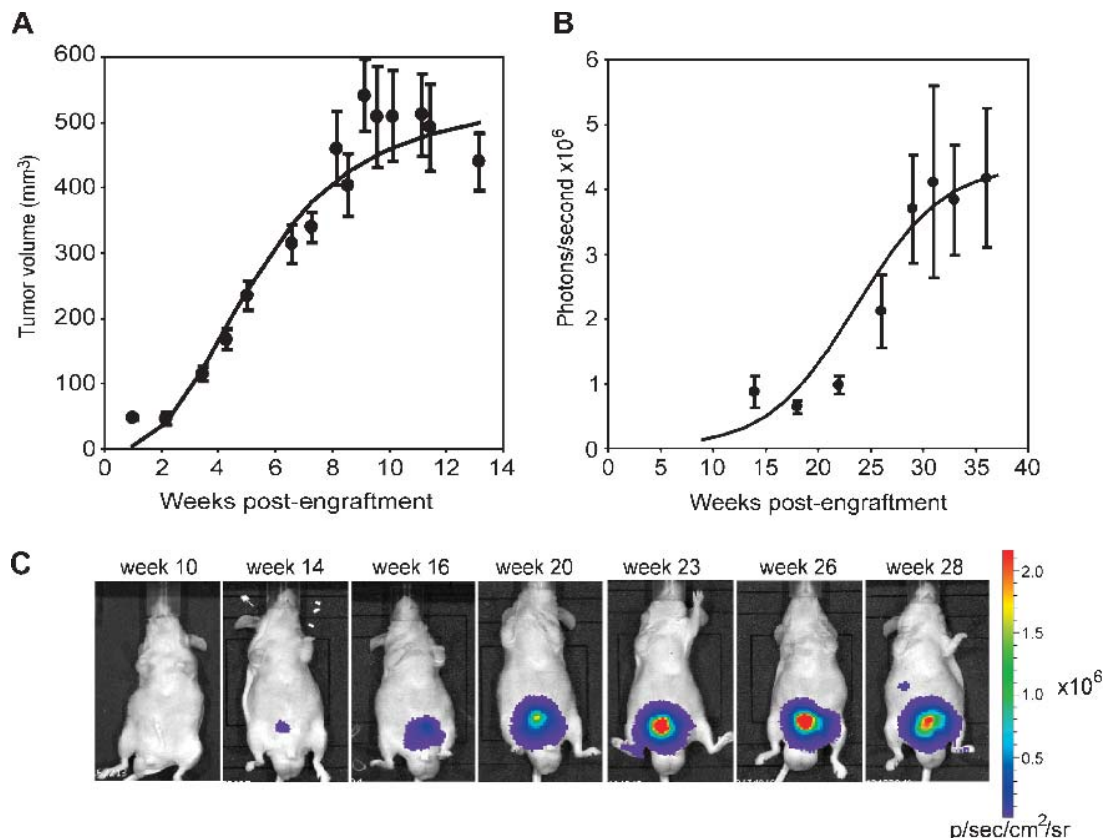


Figure 1. Progression of IGR-CaP1 tumors in animals. (A) Tumor progression of subcutaneously implanted IGR-CaP1 cells in nude mice ($n = 20$). Tumor growth was monitored weekly using caliper measurement. (B) Bioluminescent imaging time course of orthotopically inoculated GFP- and luciferase-expressing IGR-CaP1 cells. Nine mice were imaged monthly to monitor tumor growth. For A and B, the curves correspond to the adjustment of the logistic regression model on the average of the observed values at each time point, and results are expressed as the mean \pm SEM. (C) A representative mouse with intraprostatic tumor monitored by BLI showing a metastatic site at week 28.

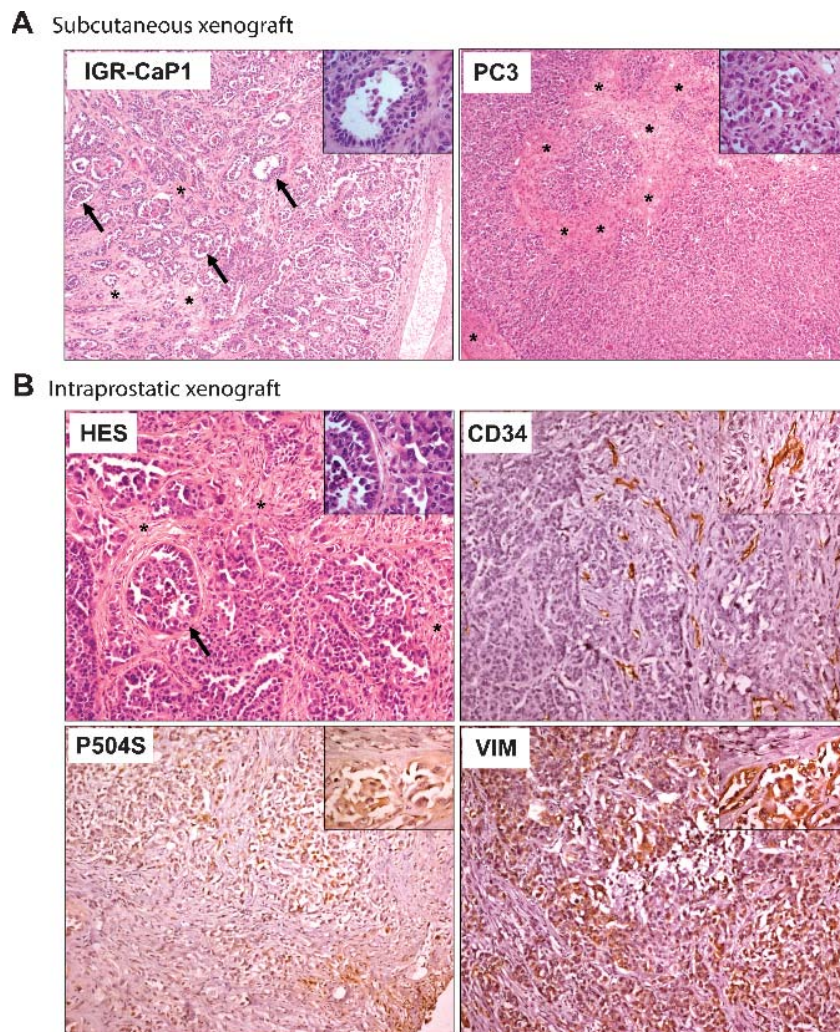


Figure 2. IGR-CaP1 tumors reconstitute prostate adenocarcinoma. IGR-CaP1 cells were injected into mice both subcutaneously (A) or intraprostatically (B). Magnification, $\times 50$; insert, $\times 400$. (A) Comparison of HES staining of tumor sections between IGR-CaP1 and PC-3 tumors revealed a glandular differentiation with acini (shown with arrows and in insert) in IGR-CaP1 tumor that is absent in PC-3 tumors. (B) HES staining of tumor sections of orthotopically implanted IGR-CaP1 cells showed more undifferentiated tumors with abundant stroma. Immunohistochemical staining of the endothelial cell marker CD34 showed a high microvessel density within the stromal regions. Vimentin (VIM) revealed the invasive potential of the tumor. Markers corresponding to AMACR (P504S) confirmed the prostate origin of the tumor. Magnification, $\times 100$; inserts, $\times 400$. Arrows indicate the presence of acini and asterisks show stromal regions.

differentiated carcinoma with a high Gleason score (Figure 2B). The endothelial cell marker CD34 was used to determine microvessel density of the tumor [22]. As shown using CD34 immunohistochemical staining, the IGR-CaP1 tumors were highly vascularized. The CD34 labeling was heterogeneous and mostly localized in the stromal areas (Figure 2B). Immunostaining for CD34 was previously observed in prostate tumors, reflecting an increased density of capillaries in invasive prostate cancer [23]. The tumorigenicity of IGR-CaP1 tumors, which was previously shown with Ki67 proliferation marker [19], was confirmed by strong expression of the vimentin invasion marker, which was mainly detected in poorly differentiated prostate cancer and bone metastases [24]. Labeling of epithelial cells with the prostate markers corresponding to P504S/AMACR confirmed the prostate origin of the tumor (Figure 2B). Taken together, the IGR-CaP1 tumors recapitulated the characteristics of aggressive prostate adenocarcinoma with a microenvironment similar to its human counterpart.

IGR-CaP1 Metastases Spread to Soft Organs

IGR-CaP1 cells formed tumors with high incidence either when administered subcutaneously or when orthotopically implanted in intact or castrated athymic male mice [19]. Although detected at low frequency, both subcutaneously and orthotopically injected IGR-CaP1 cells disseminated to distant organs, such as liver (20%, 2/10 mice), lung (20%, 2/10 mice), and the kidney and peritoneal cavity (40%, 4/10 mice) and were confirmed histologically. Figure 3A shows a large metastasis found in the liver with a weak expression of the prostate marker P504S and strong expression of vimentin. A small metastasis in the lung with high vimentin expression is also shown (Figure 3B). Because the matrix metalloproteinase (MMP-9) is critical for the formation of the metastatic niche [25], we assessed MMP-9 expression in IGR-CaP1 metastases. As shown in Figure 3A, we observed high expression of MMP-9 in the liver metastasis. Thus, this result is consistent with previous data showing that increased expression of MMP-9

is associated with higher-grade local PCa, disease recurrence, and metastatic PCa [26,27].

Intensive Bone Remodeling after Direct Injection into Bone

Bone is the main site of metastases of PCa. Compared with lesions observed in lung or breast cancer, PCa bone metastases are mainly osteoblastic. However, high bone turnover and consequent excess bone resorption are also characteristic features [28]. We evaluated the ability of the luciferase-expressing IGR-CaP1 cells to generate bone metastases using BLI and high-resolution CT. We did not detect spontaneous metastases in bone from subcutaneous or orthotopic IGR-CaP1 xenografts up to 10 months after engraftment. However, after direct intraosseous implantation of luciferase-expressing IGR-CaP1 cells into the tibia, we observed major bone lesions 10 weeks after injection in 86% of mice (6/7), visualized with three-dimensional isosurface renderings from CT scan (Figure 4A, left). Study of the individual slices confirmed bone remodeling in the injected tibias compared

with control tibias (Figure 4A, right). Indeed, the sagittal views consistently showed both lytic lesions in the cortical bone and osteoblastic lesions in the trabecular bone. SPECT using radionuclides is used to investigate bone metastases in PCa patients and provides detailed information about the anatomy and physiologic state of the bone. Bone SPECT with ^{99m}Tc -MDP is the initial method of choice to detect skeletal metastases in cancer patients [29]. ^{99m}Tc -MDP accumulates in the bone by chemical adsorption and incorporation into the hydroxyapatite structure [30]. The uptake of ^{99m}Tc -MDP was investigated after direct injection of IGR-CaP1 cells in the tibia and confirmed the mixed nature of the lesions and the intensive bone remodeling, with enhanced osteoblastic activity as indicated by a ~five-fold increase in ^{99m}Tc -MDP fixation in injected tibia *versus* control tibia (Mann-Whitney *U* test, $P = .0079$; Figure 4B). Histologic examination showed a massive invasion of cortical bone with tumor cells in the injected tibia compared with the control tibia as confirmed by HES- and trichrome-stained sections (Figure 4C). Vimentin-stained sections

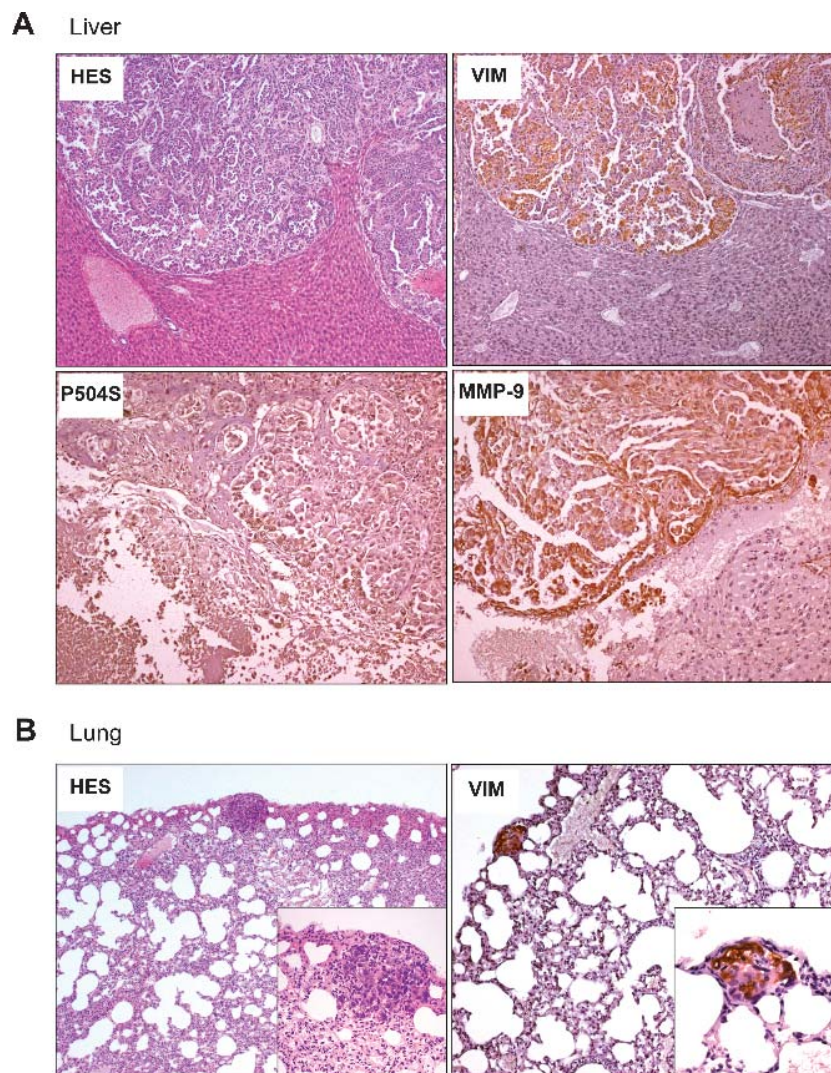


Figure 3. IGR-CaP1 tumors spontaneously disseminate to soft organs. Spontaneous metastases were observed in several organs, at week 31 after inoculation, as illustrated in the liver (A) and the lung (B). Metastases showed conserved expressions of invasive markers VIM and MMP-9. The prostate marker P504S was also conserved in the metastases. Magnifications: A, $\times 100$. B, HES, $\times 50$; insert, $\times 200$; Vim, $\times 100$; insert, $\times 400$.

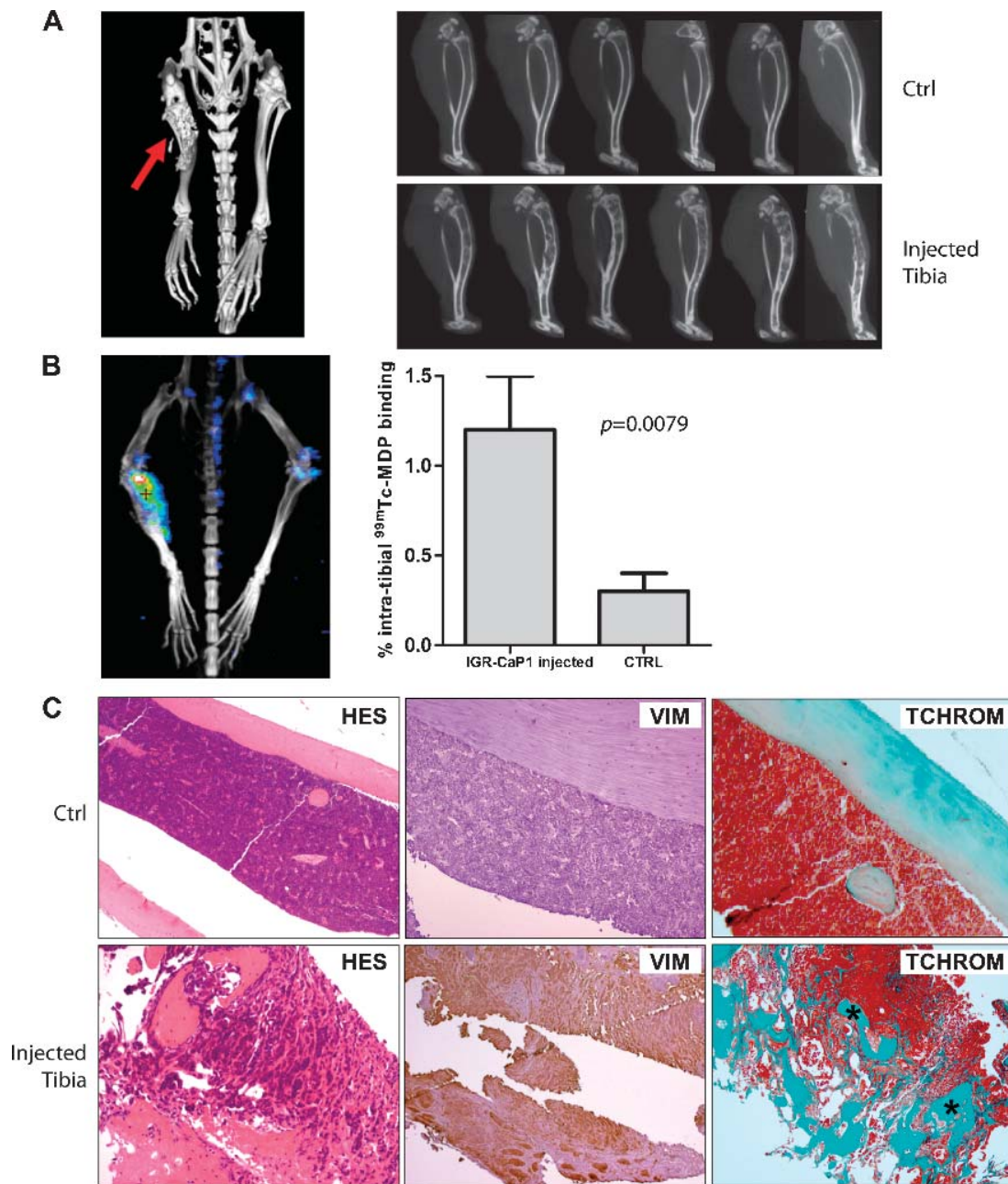


Figure 4. High levels of bone remodeling after direct injection of IGR-CaP1 cells into bone. IGR-CaP1 cells were injected into the bone marrow of the mice. (A) Massive bone remodeling (arrow) was observed by CT 5 weeks after injection of IGR-CaP1 cells in the injected tibia compared with the control noninjected tibia in 86% of mice and showed both osteolytic and osteoblastic activities. (B) The intense bone remodeling was confirmed using SPECT by measuring the incorporation of ^{99m}Tc -MDP into the bone. Quantization of the relative incorporation is shown (Mann-Whitney U test, $P = .0079$; $n = 5$). (C) Comparison of the injected tibia *versus* the control tibia by immunohistochemical staining is shown. HES staining and Masson blue trichrome staining show the remodeling within the bone marrow, visualizing newly synthesized osteoid (*). The expression of the invasive marker VIM was found both within the primary tumor and within the metastases. Magnification, $\times 100$.

confirmed the presence of the tumor cells within the bone. The mixed bone lesions were confirmed by the presence of both bone-resorbing osteoclasts on the surface of newly deposited bone (Figure W1, A and B) and the border of small osteoblasts lining bone trabeculae (Figure W1, C and D). These results are in contrast with the widely used PC-3 preclinical model, which shows exclusively osteolytic activity after bone injection [7,11,12]. Thus, the IGR-CaP1 cells were able to

generate bone lesions that closely resemble, at the bioimaging and histopathologic level, prostate tumor bone metastases that are commonly encountered clinically.

Experimental IGR-CaP1 Bone Metastases

We examined the ability of luciferase-expressing IGR-CaP1 cells to metastasize to bone using direct intracardiac injection of tumor cells

through the left cardiac ventricle in nude mice. This approach models the hematogenous dissemination of cancer cells and allows examination of the process of metastatic colonization at various organ sites. After their initial adhesion at the distant organ site, the disseminated tumor cells must proliferate sufficiently to be detectable by BLI. The bioluminescence was evaluated 5 weeks after inoculation. We eval-

uated the ability of the tumor cells to generate bone metastases using BLI, CT scan, and ^{99m}Tc -MDP SPECT. Only those mice that showed BLI signals at 5 weeks (5/9 mice) were selected for CT scan and SPECT evaluation. Bioluminescence imaging revealed metastatic colonization in bone, mostly in the mandible, femur, tibia, and vertebral column. Representative mice (Figure 5A) show the different localization of

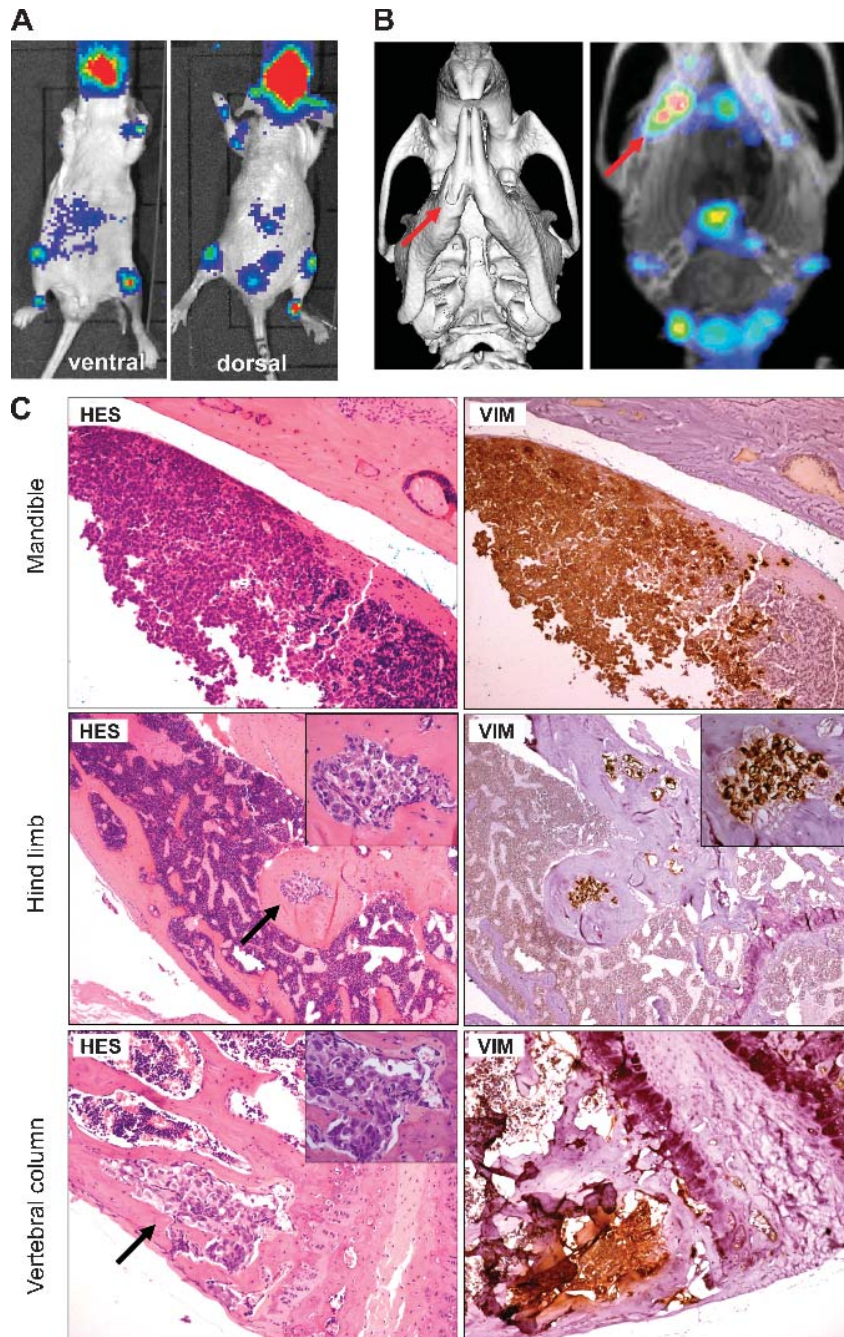


Figure 5. IGR-CaP1 cells generate bone metastases after intracardiac injections. IGR-CaP1 cells were injected into the left cardiac ventricle. (A) Multiple bone metastases were observed using BLI 5 weeks after injection. A representative mouse showed the bone localization of metastases. (B) CT scan acquisition and the incorporation of ^{99m}Tc -MDP measured with SPECT confirmed the presence of bone metastases in the mandible. (C) Histologic staining of decalcified bone sections confirmed the presence of bone lesions. As shown with intratibial injection, metastases in limb were osteoblastic. All bone metastases showed intense VIM expression. Magnification, $\times 50$; insert, $\times 400$. Arrows show the metastases.

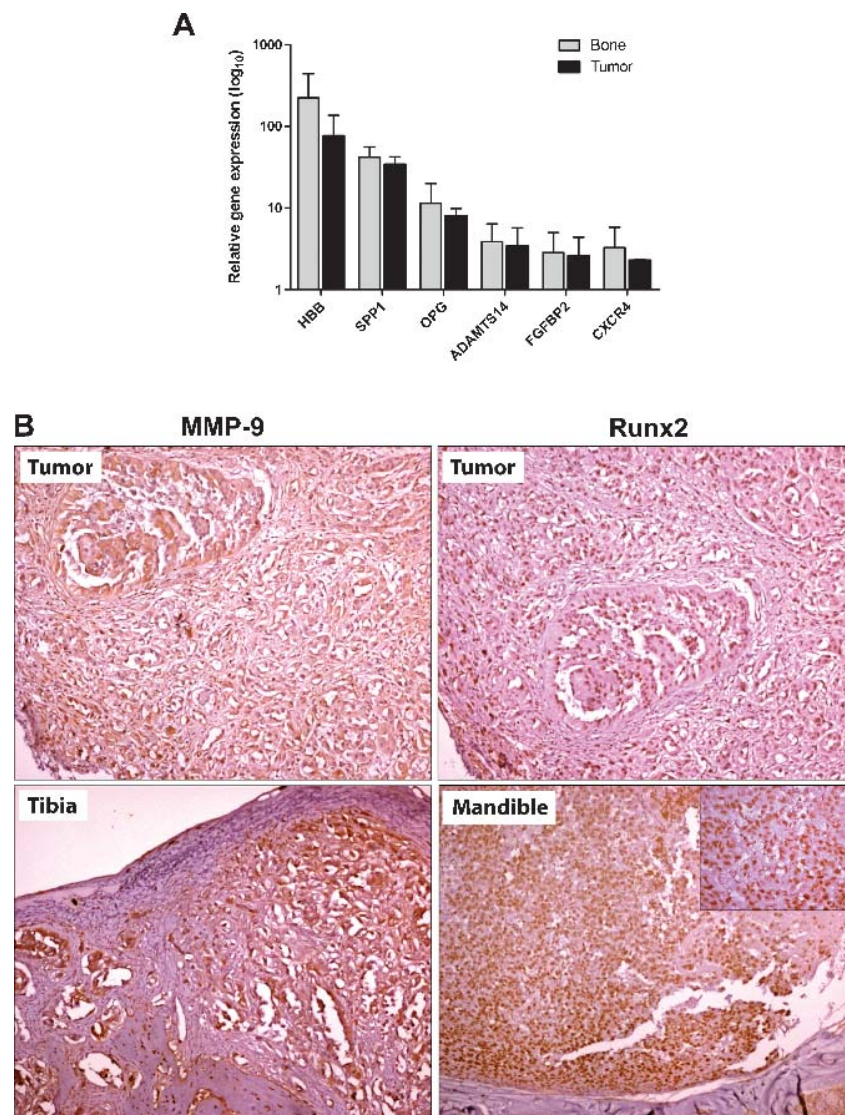


Figure 6. The IGR-CaP1 model expresses a set of human bone metastasis genes. (A) The relative expression of specific human bone metastasis genes in bone lesions was determined using real-time quantitative RT-PCR. Gene expression was detected in IGR-CaP1-injected tibias ($n = 7$; gray bars) and IGR-CaP1-xenografted tumors ($n = 4$; black bars) but not in PBS-injected control tibias. The results were normalized using the human *GAPDH* gene and were expressed relative to the universal reference RNA. (B) Immunohistochemical staining showing expression of intracellular MMP-9 and nuclear Runx2 in either intraprostatic tumors (upper figures) or decalcified bone sections (lower figures). Magnification, $\times 100$; insert, $\times 400$.

luminescence. The modification of the bone structure in the mandible was observed using CT scan (Figure 5B, left), and uptake of ^{99m}Tc -MDP revealed a two-fold increase in bone remodeling activity in the altered side of the mandible (Figure 5B, right). Histologic analysis confirmed the invasion of tumor cells in the mandible, the hind limb, and the vertebral column (Figure 5C). The osteoblastic activity of IGR-CaP1 cells was clearly evidenced in the hind limb, showing large regions of newly woven bone. Osteoclastic activity was evidenced by the presence of osteoclasts (Figure W2). All IGR-CaP1 tumor cells retained a high expression of vimentin in the bone metastases (Figure 5C). In total, all mice injected with luciferase-expressing IGR-CaP1 cells that were imaged showed metastases in bone. Taken together, these results indicate that intracardiac inoculation of luciferase-expressing IGR-CaP1 cells is a relevant model for studying homing of PCa cells and is a rare model that can target mixed osteolytic/osteoblastic bone metastases.

Specific Human Bone Metastasis Signature in IGR-CaP1 Model

Once established in bone, tumor cells interact with the bone micro-environment in a reciprocal fashion via cytokine mediators to form osteoblastic, osteolytic, or mixed lytic/blastoc lesions. We determined the expression of several genes that are frequently associated with bone metastases in breast and prostate cancer to evaluate the relevance of IGR-CaP1 as a model of human PCa bone metastases [31–34]. Gene expression was determined using real-time quantitative RT-PCR on total RNA directly extracted from IGR-CaP1-injected and control PBS-injected tibias of nude mice and from subcutaneously xenografted tumors. We were able to detect an increased gene expression of the hemoglobin B (*HBB*), *osteopontin* (*SPP1*), *OPG*, *ADAMTS14*, and *FGFBP2* human genes in IGR-CaP1-injected tibias and in tumors (Figure 6A). None of these genes were expressed in the control

PBS-injected tibias. *ADAMTS14* was slightly underexpressed in the parental IGR-CaP1 cell line (data not shown), whereas *OPG* was highly up-regulated in mice-injected cells compared with the cell line level. *HBB* and *FGFBP2* were expressed at very low levels in IGR-CaP1 (data not shown) and were highly overexpressed in bone and in tumors. These genes were previously shown to be upregulated in metastatic PCa samples [33–35]. Indeed, *osteopontin* (*SPP1*) was recently shown as a prometastasis invasion gene in human PCa and belongs to the four-gene signature of drivers of PCa progression [36]. *SPP1* was found to be highly expressed in bone and tumors (Figure 6A) and in IGR-CaP1 cells (data not shown). Because the *CXCR4/CXCL12* signaling pathway plays a pivotal role in the process of distant site metastasis and because we have previously shown that the IGR-CaP1 cells expressed *CXCR4* [19], we also measured the expression of the *CXCR4* gene in IGR-CaP1-injected bone and tumors using RT-PCR (Figure 6A). We detected *CXCR4* expression in both bone lesions and tumors. However, the expression was not significantly different between these two tissues. Furthermore, given the essential role of the transcription factor *Runx2* in osteogenesis and bone metastasis [37,38], we assessed the expression level of *Runx2* in our IGR-CaP1 mouse model using an immunohistochemical approach. Because *Runx2* directly activates the transcription of genes encoding enzymes such as *MMP-9*, we also assessed the expression of *MMP-9* in intraprostatic tumors and bone metastases by immunohistochemistry. Although the expression levels of *MMP-9* and *Runx2* were close to the limit of detection by quantitative RT-PCR in tissues, we clearly measured a high expression level of *Runx2* and *MMP-9* proteins in both intraprostatic IGR-CaP1 tumors (86% and 100%, respectively) and bone metastases (63% and 67%, respectively; Figure 6B).

Taken together, these results show that IGR-CaP1 bone metastases express a bone metastasis gene signature (*Runx2*, *CXCR4*, *MMP-9*, *HBB*, *SPP1*, *ADAMTS14*, *FGFBP2*, and *OPG*). These genes were all expressed in the parental cell line and in the primary tumors, and their expression was moderately increased in response to the bone microenvironment. On the basis of the essential role of *Runx2* in bone metastasis, our results suggest that *Runx2* may influence both osteoblastic and osteoclastic activities at the tumor-bone interface by modulating target genes.

Discussion

In the present study, we used the new prostate cell line IGR-CaP1, which was derived from primary epithelial PCa that had been previously characterized *in vitro* [19]. These cells correspond to androgen-independent basal epithelial PCa cells that exhibit high levels of cancer stem cell markers, namely *CD44*, *CD133*, and *CXCR4*. The experiments presented here detail the IGR-CaP1 animal model. IGR-CaP1 tumors grew in nude mice that were either subcutaneously injected or orthotopically implanted. The growth rate was relatively slow, with a tumor volume of $\sim 300 \text{ mm}^3$ at 6 weeks after subcutaneous implantation. In contrast with the androgen-independent PC-3 model, the IGR-CaP1 tumors exhibited glandular acini-like structures and were highly vascularized with abundant stroma, closely resembling the prostate adenocarcinoma. We observed expression of prostate-specific markers, confirming the prostate origin of the intraprostatic tumors and expression of vimentin, which is seen both in primary tumors and in metastases, revealing the invasive potential of the tumor cells. Transduction of these cells with a luciferase- and GFP-expressing retrovirus allowed the detection of spontaneous metastases in liver, lung, and/or peritoneum, albeit at a low frequency. Bioluminescence

imaging was used to follow the tumor growth of IGR-CaP1 cells injected into the prostate, bone, or heart. The tumor take, which was calculated from all the operated mice, was observed in 100% of the subcutaneous xenografts. We obtained a slightly lower tumor take depending on the technical difficulties to perform surgery for intraprostatic or intracardiac transplantations (84% and 86%, respectively).

Skeletal metastases comprise the major localization of metastatic spread in PCa. In contrast to most metastatic skeletal lesions, which are primarily osteolytic in nature, PCa metastases to bone are generally considered to be osteoblastic and are characterized by deposition of dense sclerotic bone. The study of the molecular mechanisms underlying the development of osteoblastic lesions requires cellular models that can generate osteoblastic lesions in animal models. However, there are few animal models that recapitulate spontaneous clinical bone metastases [39]. Among them, the widely used androgen-independent PC-3 model, for which luciferase-expressing versions are available, generates pure osteoclastic bone lesions. The fact that bone lesions generated by PC-3 cells do not include osteoblastic activity is an obvious limitation of this model. Other models showing osteoblastic or mixed lytic/blastic lesions when implanted in the bones of immunocompromised mice, in particular the LAPC9 and C4-2B models, have been used to study the complex interactions among the tumor cells and the bone microenvironment [9,10,40,41]. However, the fact that LAPC9 does not grow *in vitro* and needs for continued transplantation in animals is a limitation of this model. The metastatic potential of the C4-2B derived subline was artificially obtained by multiple passaging and cocultures from the LNCaP cell line. To date, the 22RV1 cell line is the unique cell line generating mixed lytic/osteoblastic bone lesions, which has been genetically modified to express luciferase, thus allowing the follow-up of bone lesions by BLI [13,14]. However, the 22RV1 cells were also obtained artificially *in vitro* from a coculture of the derived CWR22R subline, which was issued from the CWR22 xenograft [42]. In contrast, the IGR-CaP1 model, directly derived from a primary PCa, generates mixed lytic/osteoblastic bone lesions. The limitation of our model consists of the lack of detection of spontaneous bone metastases from the intraprostatic tumor in nude mice. Because bone metastases appeared at the late stages of the disease in humans, we could hypothesize that the time required for the metastatic cell spreading from the intraprostatic tumor is a long process that cannot be reached during the time course of this experiment in our animal model. The use of more immunocompromised host mice, such as *Rag2^{-/-};γc^{-/-}* mice, could be another option to circumvent this important issue. We showed in this study that the IGR-CaP1 model provides a new model of androgen-independent metastatic PCa that closely mimics the bone metastases of patients. Bone lesions and large new bone deposits were confirmed using both CT and quantitative SPECT imaging modalities. Osteolytic activity was confirmed by the presence of osteoclasts in the bone lesions. Because the bone lesions derived after intratibial implantation model may not exhibit the same biologic activity as bone metastases, intracardiac inoculation of IGR-CaP1 cells was performed and was shown to generate bone lesions with a mixed pattern. The IGR-CaP1 preclinical model is therefore a unique model obtained from a primary prostate tumor, which generates experimental bone metastasis. The establishment of a bioluminescent version of this model provides a valuable tool for the study of both intraprostatic and bone metastatic progression.

Recently, Müller et al. [43] have shown that chemokine receptors are critical in determining the metastatic destination of tumor cells. *CXCR4* is a well-known chemokine receptor that can trigger metastasis

in a variety of cancers [44,45], including PCa [46,47]. We showed previously using FACS analysis that the IGR-CaP1 cells expressed a high level of CXCR4 protein [19]. This finding is suggestive of the propensity of IGR-CaP1 cells to metastasize to bone. We have shown previously that expression of CXCR4 was indeed increased after engraftment in mice and subsequent *in vitro* culture reestablishment [19]. Previous studies have shown that CXCR4 expression correlates with the promotion of metastasis in prostate tumors [47], but contradictory results were obtained regarding the detection of CXCR4 in prostate primary tumors and metastases. These conflicting results may be due to the use of different CXCR4-directed antibodies. We were unable to detect any relevant signals by immunohistochemistry of CXCR4 in bone metastases, which may be attributed either to the low quality of available antibodies or to the decalcification procedure. However, we detected expression of the *CXCR4* gene in human tumor cells after direct-bone injection, suggesting that the attachment of primary tumor cells to basement membranes could be enhanced by CXCR4 signaling. In addition, MMPs have been reported to facilitate cancer cell invasion and metastasis through degradation of the surrounding extracellular matrix proteins. MMP expression was increased in malignant breast and PCa cells, and MMP-2 and MMP-9, in particular, have been associated with poor prognosis [48]. Recent results suggested that MMPs could be downstream targets of CXCR4-mediated signaling [49,50]. Because we observed high levels of MMP-9 protein in IGR-CaP1 tumors and bone metastases, our results suggest that MMP-9 expression may be regulated by CXCR4 expression in our model.

Once established in bone, crosstalk between tumor cells and the bone microenvironment causes impairment in the remodeling process, causing metastatic tumor cells to secrete factors that stimulate osteoclast-mediated bone destruction. Osteoblasts are also intimately involved in the regulation of osteoclast differentiation via RANKL and OPG expression. The mechanism through which IGR-CaP1 cells produces mixed osteoblastic/lytic lesions is not currently defined. However, our results suggest that the increased expression of OPG and osteopontin (SPP1) may lead to an overall inhibition of osteoclast activity, resulting in a shift of bone remodeling toward osteoblastic activity and mineralization of the bone. The role of the HBB, ADAMTS14, and FGF2 were less known, but gene expression profiles of PCa comparing expression levels between metastatic and primary tumor samples showed increased expression of these genes in metastases [33]. The effects of the overexpression of HBB and FGF2 in tissues compared with the parental IGR-CaP1 cell line need further investigations.

Runx2, a protein previously known for its master regulatory roles in the chondro-osteoblast lineage, is now emerging as a prometastatic transcription factor that may control multiple aspects of metastasis. Runx2 is expressed in androgen-independent PC-3 cells [51]. A recent study reports that Runx2 is as a key regulator of events associated with PCa metastatic bone disease by promoting activation of metastatic target genes including *VEGF*, *osteopontin*, *MMPs*, and *survivin* [52]. As was previously described in human PCa tissues, we observed high immunohistochemical expression of Runx2 in aggressive intraprostatic tumors and bone metastases. The high expression of Runx2 protein in bone metastases in the IGR-CaP1 preclinical model suggests that Runx2 might be implicated in the regulation of osteopontin and MMP-9. Our results suggest that the Runx2-mediated pathway may be implicated in the osteoblastic properties of the IGR-CaP1 bone lesions.

This article describes a new preclinical model of PCa in immunocompromised mice, which experimentally reproduces the widespread

bone metastasis with mixed osteolytic/blastic lesions that is often observed in patients. Dynamic monitoring was used to follow the metastatic dissemination using noninvasive bioluminescence, CT, and quantitative SPECT imaging modalities. We also provided an expression signature for the responsiveness of IGR-CaP1 cells to the bone microenvironment, namely *CXCR4*, *MMP-9*, *Runx2*, *osteopontin*, *OPG*, *ADAMTS14*, *FGF2*, and *HBB* expression, suggesting that a combination of therapeutic approaches for targeting both osteoblasts and osteoclasts may be beneficial in limiting the progression of established bone metastasis. Therefore, the IGR-CaP1 model is one of the few suitable models for preclinical studies providing osteosclerotic bone changes and for *in vitro* studies in tissue culture and three-dimensional spheroids. The up-regulation of the proteins corresponding to the bone metastasis signature suggests potential targets for reversing bone metastasis; these mechanisms could be studied using the IGR-CaP1 preclinical model to elucidate drug targets with potential clinical relevance.

Acknowledgments

The authors thank S. Cotteret for the critical reading of the article and J.L. Villeval, J.P. Morgenstern, and X. Xiong for the kind gift of the luciferase-GFP expression retroviral vector. The authors also thank J. Sobilo and S. Retif for technical help, G. Reveillon for his help with the CT and SPECT quantifications, and F. Commo for his help with the statistical analysis.

References

- [1] Jemal A, Siegel R, Xu J, and Ward E (2010). Cancer statistics, 2010. *CA Cancer J Clin* **60**, 277–300.
- [2] Chevillet JC, Tindall D, Boelter C, Jenkins R, Lohse CM, Pankratz VS, Sebo TJ, Davis B, and Blute ML (2002). Metastatic prostate carcinoma to bone: clinical and pathologic features associated with cancer-specific survival. *Cancer* **95**, 1028–1036.
- [3] Mundy GR (2002). Metastasis to bone: causes, consequences and therapeutic opportunities. *Nat Rev Cancer* **2**, 584–593.
- [4] Roodman GD (2004). Mechanisms of bone metastasis. *N Engl J Med* **350**, 1655–1664.
- [5] Jin J-K, Dayyani F, and Gallick GE (2011). Steps in prostate cancer progression that lead to bone metastasis. *Int J Cancer* **128**, 2545–2561.
- [6] Seibel MJ (2005). Clinical use of markers of bone turnover in metastatic bone disease. *Nat Clin Pract Oncol* **2**, 504–517.
- [7] Nemeth JA, Yousif R, Herzog M, Che M, Upadhyay J, Shekarriz B, Bhagat S, Mullins C, Fridman R, and Cher ML (2002). Matrix metalloproteinase activity, bone matrix turnover, and tumor cell proliferation in prostate cancer bone metastasis. *J Natl Cancer Inst* **94**, 17–25.
- [8] Wu TT, Sikes RA, Cui Q, Thalmann GN, Kao C, Murphy CF, Yang H, Zhou HE, Balian G, and Chung LW (1998). Establishing human prostate cancer cell xenografts in bone: induction of osteoblastic reaction by prostate-specific antigen-producing tumors in athymic and SCID/bg mice using LNCaP and lineage-derived metastatic sublines. *Int J Cancer* **77**, 887–894.
- [9] Hall CL, Bafico A, Dai J, Aaronson SA, and Keller ET (2005). Prostate cancer cells promote osteoblastic bone metastases through Wnts. *Cancer Res* **65**, 7554–7560.
- [10] Hsu WK, Virk MS, Feeley BT, Stout DB, Chatziioannou AF, and Lieberman JR (2008). Characterization of osteolytic, osteoblastic, and mixed lesions in a prostate cancer mouse model using ¹⁸F-FDG and ¹⁸F-fluoride PET/CT. *J Nucl Med* **49**, 414–421.
- [11] Corey E, Quinn JE, Bladou F, Brown LG, Roudier MP, Brown JM, Buhler KR, and Vessella RL (2002). Establishment and characterization of osseous prostate cancer models: intra-tibial injection of human prostate cancer cells. *Prostate* **52**, 20–33.
- [12] Lee Y-P, Schwarz EM, Davies M, Jo M, Gates J, Zhang X, Wu J, and Lieberman JR (2002). Use of zoledronate to treat osteoblastic versus osteolytic lesions in a severe-combined-immunodeficient mouse model. *Cancer Res* **62**, 5564–5570.
- [13] Henry MD, Silva MD, Wen S, Siebert E, Solin E, Chandra S, and Worland PJ (2005). Spiculated periosteal response induced by intraosseous injection of 22Rv1

- prostate cancer cells resembles subset of bone metastases in prostate cancer patients. *Prostate* **65**, 347–354.
- [14] Drake JM, Gabriel CL, and Henry MD (2005). Assessing tumor growth and distribution in a model of prostate cancer metastasis using bioluminescence imaging. *Clin Exp Metastasis* **22**, 674–684.
- [15] Fizazi K, Sikes CR, Kim J, Yang J, Martinez LA, Olive MC, Logothetis CJ, and Navone NM (2004). High efficacy of docetaxel with and without androgen deprivation and estramustine in preclinical models of advanced prostate cancer. *Anticancer Res* **24**, 2897–2903.
- [16] Kundra V, Ng CS, Ma J, Bankson JA, Price RE, Cody DD, Do K-A, Han L, and Navone NM (2007). *In vivo* imaging of prostate cancer involving bone in a mouse model. *Prostate* **67**, 50–60.
- [17] Li X, Loberg R, Liao J, Ying C, Snyder LA, Pienta KJ, and McCauley LK (2009). A destructive cascade mediated by CCL2 facilitates prostate cancer growth in bone. *Cancer Res* **69**, 1685–1692.
- [18] Schneider A, Kalikin LM, Mattos AC, Keller ET, Allen MJ, Pienta KJ, and McCauley LK (2005). Bone turnover mediates preferential localization of prostate cancer in the skeleton. *Endocrinology* **146**, 1727–1736.
- [19] Chauchereau A, Al Nakouzi N, Gaudin C, Le Moulec S, Compagno D, Auger N, Bénard J, Opolon P, Rozet F, Validire P, et al. (2011). Stemness markers characterize IGR-CaP1, a new cell line derived from primary epithelial prostate cancer. *Exp Cell Res* **317**, 262–275.
- [20] Morgenstern JP and Land H (1990). Advanced mammalian gene transfer: high titre retroviral vectors with multiple drug selection markers and a complementary helper-free packaging cell line. *Nucleic Acids Res* **18**, 3587–3596.
- [21] Singh AS and Figg WD (2005). *In vivo* models of prostate cancer metastasis to bone. *J Urol* **174**, 820–826.
- [22] Rössler J, Monnet Y, Farace F, Opolon P, Daudigeos-Dubus E, Bourredjem A, Vassal G, and Geoerger B (2011). The selective VEGFR1-3 inhibitor axitinib (AG-013736) shows antitumor activity in human neuroblastoma xenografts. *Int J Cancer* **128**, 2748–2758.
- [23] Bettencourt MC, Bauer JJ, Sesterhenn IA, Connelly RR, and Moul JW (1998). CD34 immunohistochemical assessment of angiogenesis as a prognostic marker for prostate cancer recurrence after radical prostatectomy. *J Urol* **160**, 459–465.
- [24] Lang SH, Hyde C, Reid IN, Hitchcock IS, Hart CA, Bryden AAG, Villette J-M, Stower MJ, and Maitland NJ (2002). Enhanced expression of vimentin in motile prostate cell lines and in poorly differentiated and metastatic prostate carcinoma. *Prostate* **52**, 253–263.
- [25] Kessenbrock K, Plaks V, and Werb Z (2010). Matrix metalloproteinases: regulators of the tumor microenvironment. *Cell* **141**, 52–67.
- [26] Zhang L, Shi J, Feng J, Klocker H, Lee C, and Zhang J (2004). Type IV collagenase (matrix metalloproteinase-2 and -9) in prostate cancer. *Prostate Cancer Prostatic Dis* **7**, 327–332.
- [27] Trudel D, Fradet Y, Meyer F, and Têtu B (2010). Matrix metalloproteinase 9 is associated with Gleason score in prostate cancer but not with prognosis. *Hum Pathol* **41**, 1694–1701.
- [28] Yi B, Williams PJ, Niewolna M, Wang Y, and Yoneda T (2002). Tumor-derived platelet-derived growth factor-BB plays a critical role in osteosclerotic bone metastasis in an animal model of human breast cancer. *Cancer Res* **62**, 917–923.
- [29] Uematsu T, Yuen S, Yukisawa S, Aramaki T, Morimoto N, Endo M, Furukawa H, Uchida Y, and Watanabe J (2005). Comparison of FDG PET and SPECT for detection of bone metastases in breast cancer. *AJR Am J Roentgenol* **184**, 1266–1273.
- [30] Kanishi D (1993). ^{99m}Tc-MDP accumulation mechanisms in bone. *Oral Surg Oral Med Oral Pathol* **75**, 239–246.
- [31] Cawthorn TR, Amir E, Broom R, Freedman O, Gianfelice D, Barth D, Wang D, Holen I, Done SJ, and Clemons M (2009). Mechanisms and pathways of bone metastasis: challenges and pitfalls of performing molecular research on patient samples. *Clin Exp Metastasis* **26**, 935–943.
- [32] Kang Y, Siegel PM, Shu W, Drobnyak M, Kakonen SM, Córdón-Cardo C, Guise TA, and Massagué J (2003). A multigenic program mediating breast cancer metastasis to bone. *Cancer Cell* **3**, 537–549.
- [33] Chandran UR, Ma C, Dhir R, Bisceglia M, Lyons-Weiler M, Liang W, Michalopoulos G, Becich M, and Monzon FA (2007). Gene expression profiles of prostate cancer reveal involvement of multiple molecular pathways in the metastatic process. *BMC Cancer* **7**, 64.
- [34] Chen G, Sircar K, Aprikian A, Potti A, Goltzman D, and Rabbani SA (2006). Expression of RANKL/RANK/OPG in primary and metastatic human prostate cancer as markers of disease stage and functional regulation. *Cancer* **107**, 289–298.
- [35] Lin DL, Tarnowski CP, Zhang J, Dai J, Rohn E, Patel AH, Morris MD, and Keller ET (2001). Bone metastatic LNCaP-derivative C4-2B prostate cancer cell line mineralizes *in vitro*. *Prostate* **47**, 212–221.
- [36] Ding Z, Wu C-J, Chu GC, Xiao Y, Ho D, Zhang J, Perry SR, Labrot ES, Wu X, Lis R, et al. (2011). SMAD4-dependent barrier constrains prostate cancer growth and metastatic progression. *Nature* **470**, 269–273.
- [37] Yang J, Mani SA, Donaher JL, Ramaswamy S, Itzykson RA, Come C, Savagner P, Gitelman I, Richardson A, and Weinberg RA (2004). Twist, a master regulator of morphogenesis, plays an essential role in tumor metastasis. *Cell* **117**, 927–939.
- [38] Pratap J, Lian JB, Javed A, Barnes GL, van Wijnen AJ, Stein JL, and Stein GS (2006). Regulatory roles of Runx2 in metastatic tumor and cancer cell interactions with bone. *Cancer Metastasis Rev* **25**, 589–600.
- [39] Chauchereau A (2011). Experimental models for the development of new medical treatments in prostate cancer. *Eur J Cancer* **47**(suppl 3), S200–S214.
- [40] Feeley BT, Gamradt SC, Hsu WK, Liu N, Krenek L, Robbins P, Huard J, and Lieberman JR (2005). Influence of BMPs on the formation of osteoblastic lesions in metastatic prostate cancer. *J Bone Miner Res* **20**, 2189–2199.
- [41] Lee Y, Schwarz E, Davies M, Jo M, Gates J, Wu J, Zhang X, and Lieberman JR (2003). Differences in the cytokine profiles associated with prostate cancer cell induced osteoblastic and osteolytic lesions in bone. *J Orthop Res* **21**, 62–72.
- [42] Sramkoski RM, Pretlow TG II, Giaconia JM, Pretlow TP, Schwartz S, Sy MS, Marengo SR, Rhim JS, Zhang D, and Jacobberger JW (1999). A new human prostate carcinoma cell line, 22Rv1. *In Vitro Cell Dev Biol Anim* **35**, 403–409.
- [43] Müller A, Homey B, Soto H, Ge N, Catron D, Buchanan ME, McClanahan T, Murphy E, Yuan W, Wagner SN, et al. (2001). Involvement of chemokine receptors in breast cancer metastasis. *Nature* **410**, 50–56.
- [44] Burger JA and Kipps TJ (2006). CXCR4: a key receptor in the crosstalk between tumor cells and their microenvironment. *Blood* **107**, 1761–1767.
- [45] Kucia M, Reza R, Miekus K, Wanzeck J, Wojakowski W, Janowska-Wieczorek A, Ratajczak J, and Ratajczak MZ (2005). Trafficking of normal stem cells and metastasis of cancer stem cells involve similar mechanisms: pivotal role of the SDF-1–CXCR4 axis. *Stem Cells* **23**, 879–894.
- [46] Taichman RS, Cooper C, Keller ET, Pienta KJ, Taichman NS, and McCauley LK (2002). Use of the stromal cell–derived factor-1/CXCR4 pathway in prostate cancer metastasis to bone. *Cancer Res* **62**, 1832–1837.
- [47] Sun Y-X, Schneider A, Jung Y, Wang J, Dai J, Wang J, Cook K, Osman NI, Koh-Paige AJ, Shim H, et al. (2005). Skeletal localization and neutralization of the SDF-1(CXCL12)/CXCR4 axis blocks prostate cancer metastasis and growth in osseous sites *in vivo*. *J Bone Miner Res* **20**, 318–329.
- [48] Chabottaux V and Noel A (2007). Breast cancer progression: insights into multifaceted matrix metalloproteinases. *Clin Exp Metastasis* **24**, 647–656.
- [49] Yu T, Wu Y, Helman JJ, Wen Y, Wang C, and Li L (2011). CXCR4 promotes oral squamous cell carcinoma migration and invasion through inducing expression of MMP-9 and MMP-13 via the ERK signaling pathway. *Mol Cancer Res* **9**, 161–172.
- [50] Wang Q, Diao X, Sun J, and Chen Z (2011). Regulation of VEGF, MMP-9, and metastasis by CXCR4 in a prostate cancer cell line. *Cell Biol Int* **35**, 897–904.
- [51] Yeung F, Law WK, Yeh C-H, Westendorf JJ, Zhang Y, Wang R, Kao C, and Chung LWK (2002). Regulation of human osteocalcin promoter in hormone-independent human prostate cancer cells. *J Biol Chem* **277**, 2468–2476.
- [52] Akech J, Wixted JJ, Bedard K, van der Deen M, Hussain S, Guise TA, van Wijnen AJ, Stein JL, Languino LR, Altieri DC, et al. (2010). Runx2 association with progression of prostate cancer in patients: mechanisms mediating bone osteolysis and osteoblastic metastatic lesions. *Oncogene* **29**, 811–821.

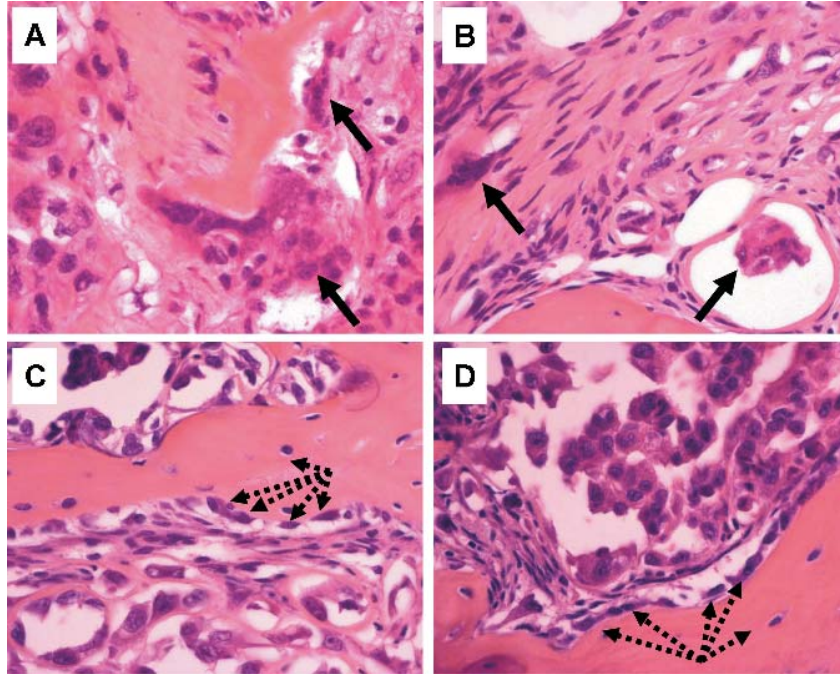


Figure W1. HES staining of the bone lesions obtained after a direct injection into the tibia showing bone remodeling. (A and B) Osteoclasts (arrows). (C and D) Osteoblasts (arrows).

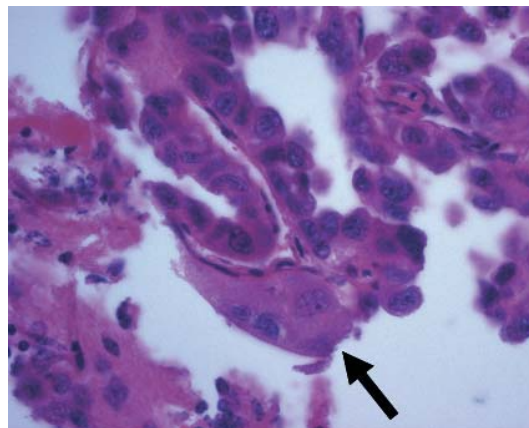


Figure W2. HES staining of the bone lesions obtained after injection of tumor cells into the left ventricle. Arrows show the presence of osteoclasts in the bone lesions.